Optimization of Triboelectric Nanogenerator Charging Systems for Efficient Energy Harvesting and Storage

Simiao Niu, Ying Liu, Yu Sheng Zhou, Sihong Wang, Long Lin, and Zhong Lin Wang

***Abstract*— Triboelectric nanogenerator (TENG) technology has emerged as a new mechanical energy harvesting technology with numerous advantages. This paper analyzes its charging behavior together with a load capacitor. Through numerical and analytical modeling, the charging performance of a TENG with a bridge rectifier under periodic external mechanical motion is completely analogous to that of a dc voltage source in series with an internal resistance. An optimum load capacitance that matches the TENGs impedance is observed for the maximum stored energy. This optimum load capacitance is theoretically detected to be linearly proportional to the charging cycle numbers and the inherent TENG capacitance. Experiments were also performed to further validate our theoretical anticipation and show the potential application of this paper in guiding real experimental designs.**

***Index Terms*— Capacitor, charging characteristics, mechanical energy harvesting, triboelectric nanogenerator (TENG).**

I. Introduction

With the rapid growth of portable electronics and sensor networks, mobile and sustainable energy sources for these devices become indispensable in modern society. In addition to the use of batteries, harvesting energy from ambient environment for powering these devices has attracted extensive attention recently. Among all of the energy sources, universally available mechanical energy has become a plausible solution. Traditional mechanical-energy-harvesting techniques have long been focused on electromagnetic [1], [2], electrostatic [3]–[7], and piezoelectric methods [8]. Recently, triboelectric nanogenerators (TENGs) based on contact electrification [9]–[11] and electrostatic induction emerge as a promising mechanical energy harvesting technique because of their unique figure of merits, including high output power density, ultrahigh energy conversion efficiency, low weight, cost-effective materials, and high adaptability design to different applications [12]–[16]. However, because of the inherent uncontrollable and unstable characteristics of environmental mechanical energy sources, the converted electrical energy from TENGs is thus unstable and hardly utilized to directly power electronic devices. Usually, storage elements such as capacitors or batteries are needed to stabilize and regulate the power output for direct application [13]. Thus, understanding the integration performance of TENGs with an energy storage unit is critical for designing a practical energy-harvesting system. However, until now there are many mysteries about the charging behavior of TENGs. First, their basic charging characteristics are not yet clear. In addition, the influence of the load capacitance and TENG parameters on the charging characteristics is still unknown. Finally, similar to a resistive load, there should be an optimum load capacitance for maximized energy storage, while a mismatch between the TENG and the load capacitance could dramatically decrease the energy storage efficiency. However, the validation of these statements and how the TENG parameters can affect this optimum load capacitance still needs to be investigated.

In this paper, the characteristics of utilizing a TENG to charge a capacitor were discussed in depth. First, the easiest unidirectional charging was analyzed to show the importance of impedance match in the design of such systems. Then, a much more complicated multicycle charging process was analyzed to show the unique TENG charging characteristics. An optimum load capacitance was observed for the maximized energy storage. To obtain the optimized design strategy for such system, the analytical solution of the optimum load capacitance was detected and its dependence on the charging cycle numbers and TENG structural parameters was shown. Finally, corresponding experiments were performed to further validate the above theoretical prediction and show its application in guiding experiments.

II. TENG Charging Performance Under Unidirectional Mechanical Motion

We start our discussion with the simplest case, which is, utilizing a single-electrode TENG to charge a load capacitor (C_L) under a unidirectional mechanical motion. In this process, no external rectifier is needed, as the charging current of the TENG is also unidirectional. In addition, the

Manuscript received July 15, 2014; revised October 25, 2014 and November 17, 2014; accepted December 1, 2014. Date of publication December 22, 2014; date of current version January 20, 2015. This work was supported in part by the U.S. Department of Energy through the Office of Basic Energy Sciences under Grant DE-FG02-07ER46394, in part by the International Center for Materials Nanoarchitectonics (MANA) through the National Institute for Materials Science, Japan, in part by the Thousand Talents Program for the Pioneer Researcher and their innovation team, China, in part by the Hightower Chair foundation, in part by Sungkyunkwan University, Korea. The review of this paper was arranged by Editor F. Ayazi.

S. Niu, Y. Liu, Y. S. Zhou, S. Wang, and L. Lin are with the School of Materials Science and Engineering, Georgia Institute of Technology, Atlanta, GA 30332 USA (e-mail: sniu6@gatech.edu; kingcythia@gmail.com; zhou.yusheng.alvin@gmail.com; wangsh05@gmail.com; linlong06@gmail.com).

Z. L. Wang is with the School of Materials Science and Engineering, Georgia Institute of Technology, Atlanta, GA 30332 USA, and also with the Beijing Institute of Nanoenergy and Nanosystems, Chinese Academy of Sciences, Beijing 100089, China (e-mail: zhong.wang@mse.gatech.edu).

Color versions of one or more of the figures in this paper are available online at http://ieeexplore.ieee.org.

Digital Object Identifier 10.1109/TED.2014.2377728

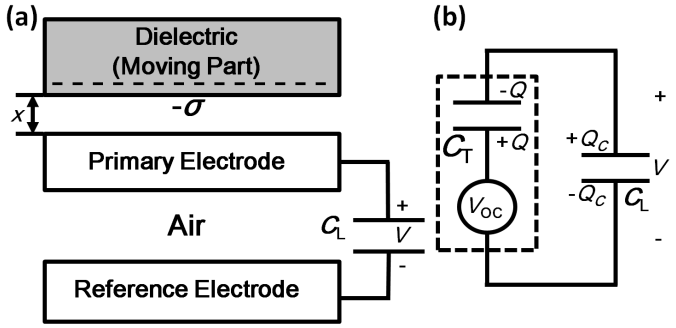

Fig. 1. (a) Structure for single-electrode TENG used in the unidirectional charging calculation. (b) Equivalent circuit model of the whole system in the unidirectional charging calculation.

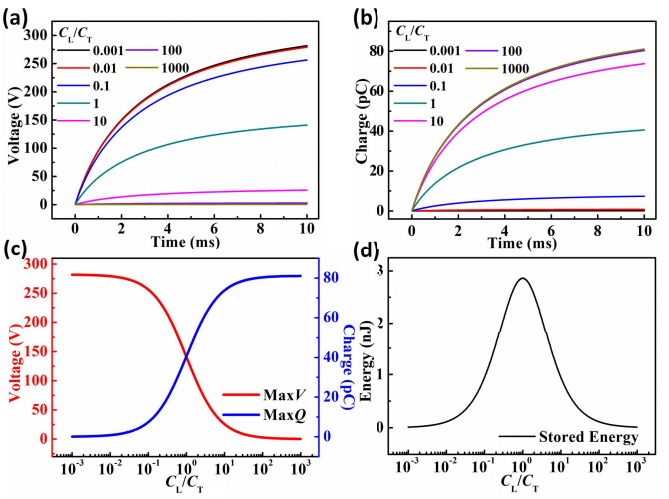

Fig. 2. TENG charging characteristics under unidirectional mechanical motion. (a) Voltage-time relationship at different load capacitances. (b) Stored charge-time relationship at different load capacitances. (c) Influence of the load capacitance on the final voltage and charge stored in the load capacitor. (d) Final stored energy profile with load capacitance.

inherent capacitance (C_T) of a single-electrode TENG is nearly constant, which will also simplify our discussion [17]. As shown in Fig. 1(a), the model of a single-electrode TENG contains a moving dielectric and two stationary electrodes (primary and reference electrodes) [17]. The dielectric and the primary electrode will undergo contact electrification. After the contact electrification, the top dielectric carries negative charges with a density of $-\sigma$ on its bottom surface and the primary electrode has the same amount of positive charges. When the dielectric and the primary electrode are vertically separated (the separation distance is defined as x), electrons will transfer from the reference electrode to the primary electrode because of the electrostatic induction. With Q defined as the transferred charges from the primary electrode to the reference electrode, the total charges on the primary electrode and the bottom electrode is $\sigma S - Q$ and Q, respectively. The charges on the top plate of the load capacitor are defined as Q^C. Thus, with the previous demonstrated equivalent circuit model of TENGs [18], the equivalent circuit diagram of the whole system can be shown [Fig. 1(b)]. In this first-order equivalent circuit model, there are no resistors included mainly because of the following three reasons.

1) The inherent TENG resistance is purposely designed to be close to infinity to maximize the power output.
2) The parasitic resistance from the metal electrode is negligible compared with the impedance of normal load conditions.
3) The mechanical motion period applied to the TENG is much smaller than the surface triboelectric charge decay time constant, so the decay of the surface triboelectric charge can also be neglected.

To solve the above equivalent circuit, the initial condition must be specified. As a typical example, we consider the case that at $t = 0$, the top dielectric has stopped at $x = 0$ position for a long time and just starts moving. In addition, no initial charges are stored on the load capacitor, so initial charges on both C_T and C_L are 0 ($Q(t = 0) = Q^C(t = 0) = 0$). Thus, the following equations can be obtained from Kirchhoff's law and node charge conservation, where V stands for the voltage across C_L and V_{OC} stands for the open circuit (OC) voltage of the TENG under minimum achievable charge reference state

$$V = -\frac{1}{C_T}Q + V_{OC} = \frac{1}{C_L}Q^C \tag{1}$$

$$Q^C - Q = Q^C(t = 0) - Q(t = 0) = 0. \tag{2}$$

In practical application, the motion of the dielectric always has a maximum separation distance, which is defined as x_{max}. Thus, the final voltage and charge on the capacitor when a full separation is reached (x reaches x_{max}) can be obtained by solving the above two equations. [$V_{OC,max}$ and $Q_{SC,max}$ stands for the OC voltage and short circuit (SC) transferred charge of the TENG when $x = x_{max}$]

$$V(x = x_{max}) = \frac{C_T V_{OC,max}}{C_L + C_T} = \frac{Q_{SC,max}}{C_L + C_T} \tag{3}$$

$$Q^C(x = x_{max}) = \frac{C_L Q_{SC,max}}{C_L + C_T}. \tag{4}$$

Thus, the total energy stored in the capacitor (E^C) can be given by

$$E^C = \frac{1}{2}C_L[V(x = x_{max})]^2 = \frac{C_L[Q_{SC}(x = x_{max})]^2}{2(C_L + C_T)^2}. \tag{5}$$

To obtain an intuitive sense of such equations, numerical calculation for the single-electrode TENG under constant velocity motion condition is performed and output profiles as a function of time with different load capacitances are shown in Fig. 2. (The detailed calculation parameters are listed in Table I.) When C_L is small, its impedance is much larger than the impedance of C_T. Thus, almost all of the V_{OC} is applied on C_L and the TENG is working under a quasi-OC condition. Therefore, as shown in Fig. 2(a), the voltage charging curves for small C_L are all close to the V_{OC} curve. However, the stored charge is still close to zero because of the small C_L, leading to a limited final stored energy. On the opposite, when C_L is very large, its impedance

TABLE I
PARAMETERS UTILIZED IN THE CALCULATION OF THE UNIDIRECTIONAL CHARGING BEHAVIORS FOR A SINGLE-ELECTRODE TENG

Relative dielectric constant ε_r	2
Thickness of the dielectric d_r	100 μm
Width of the structure w	5 mm
Length of Dielectrics l	5 mm
Gap distance between the electrodes g	1 mm
Tribo-charge surface density σ	8 μC m^{-2}
Maximum separation distance x_{max}	0.02 m
Average Velocity v	1 m/s

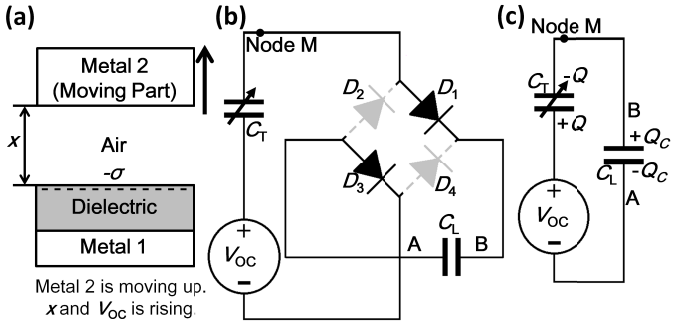

Fig. 3. Equivalent circuit diagram for TENG charging performance calculation under periodic mechanical motion. (a) Structure of the contact-mode attached-electrode TENG used in the calculation. (b) Circuit diagram showing the conduction condition of full-bridge rectifier in the first half cycle. (c) Simplified circuit diagram under ideal diode approximation in the first half cycle.

is much smaller than the impedance of C_T, so the voltage applied on C_L is approximately zero. At this moment, the TENG is working under a quasi-SC condition and the stored-charge curves for large C_L are all close to the Q_{SC} curve. However, the total stored energy is still limited because of the low voltage across C_L. From the above analysis, only at the transition region the stored energy can reach its maximum. Mathematically, it can be easily derived from (5) that the optimum load capacitance ($C_{L,opt}$) at which the maximum stored energy is reached is equal to C_T, as shown in Fig. 2(d). Physically, this means the impedance match between the TENG and the load is reached.

III. TENG CHARGING PERFORMANCE UNDER PERIODIC MECHANICAL MOTION

Above, we analyzed the charging behavior of a single-electrode TENG to charge a load capacitor under a unidirectional motion. However, in practical applications, the mechanical motion is almost never unidirectional, resulting in an ac charging current. Therefore, a full-bridge diode rectifier is necessary to prevent the charge leaking back from C_L to the TENG. In addition, the inherent capacitance of most TENGs is time-variant [20]. Therefore, the real case is much more complicated than the above discussion. As a typical example, the case we analyzed in Section III is a contact-mode attached-electrode TENG under a periodic

TABLE II
PARAMETERS UTILIZED IN THE CALCULATION OF THE MULTICYCLE CHARGING BEHAVIORS FOR A CONTACT-MODE ATTACHED-ELECTRODE TENG

Relative dielectric constant ε_r	2.1
Thickness of the dielectric d_r	50 μm
Area of the dielectric S	0.005 m^2
Tribo-charge surface density σ	40 μC m^{-2}
Maximum separation distance x_{max}	0.002 m
Average Velocity v	0.1 m/s

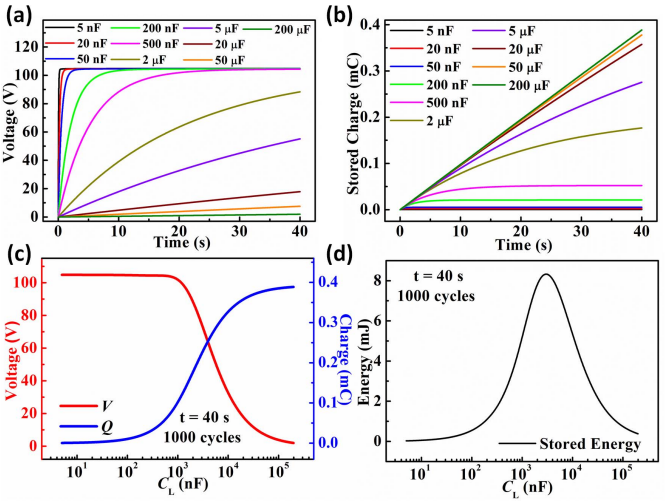

Fig. 4. TENG charging characteristics under periodic mechanical motion. (a) Voltage-time relationship at different load capacitances. (b) Stored charge-time relationship at different load capacitances. (c) Influence of the load capacitance on the final voltage and charge stored in the load capacitor. (d) Final stored energy profile with load capacitance.

harmonic motion process [21]

$$x = x_{\max}\left[\frac{1}{2} - \frac{1}{2}\cos\left(\frac{\pi v}{x_{\max}}t\right)\right]. \tag{6}$$

The structure of this TENG is shown in Fig. 3(a) and its working principle is very similar to the above single-electrode TENG [21]. Utilizing the parameters listed in Table II, we can obtain the numerical results of this nonlinear time-variant system shown in Fig. 3(b) from the TENG-simulator demonstrated in our previous work [18]. The simulation results are shown in Fig. 4. As shown in Fig. 4(a), a saturation charging curve is observed for all the load capacitors, which is very similar to a typical resistor-capacitor (RC) charging curve in shape. At $t = 0$, the load capacitor is charging at a maximum speed. Then, the charging speed gradually slows down and finally the same saturation voltage ~104.8 V is reached for all the different load capacitors. It takes less time to charge a smaller C_L to reach its saturation voltage. However, a different trend is observed for the stored charges. At beginning, the curves for all load capacitors converge to one linear curve, with the charging rate of $2Q_{SC,max}$ per cycle. However, when time increases, the curves from small C_L shift downward first and finally get saturated. At this moment, very few charges can be pumped into the capacitor. The voltage and the stored charge

of the load capacitor after 1000 charging cycles are shown in Fig. 4(c), which have the similar trend as the unidirectional charging case. When C_L is small enough, the voltage on the load capacitor is approximately its saturation voltage while the stored charges are close to zero and proportional to C_L. When C_L is large enough, the stored charges are approximately $2kQ_{\mathrm{SC,max}}$ while the voltage is close to zero and inversely proportional to C_L. Similar to the previous unidirectional charging, an optimum capacitance for maximum stored energy is also observed in the transition region of C_L.

In addition to the demonstrated numerical calculation, an analytical solution is preferred to better understand the underline physics despite the fact that only approximate solution can be derived. To address this nonlinear time-variant system, linearizing the diodes of the bridge rectifier is a critical step. As shown in Fig. 3(a) and (b), in the first half of each cycle, the top plate is moving upward and V_{oc} is increasing. Neglecting the reverse leakage current of the diode, we can assume only diode 1 and 3 are conducting in this step and diode 2 and 4 are fully open-circuit. In addition, the conducting voltage of these two diodes can be neglected, for it is much smaller than the open-circuit voltage of the TENG. With the above assumptions, the complex circuit shown in Fig. 3(b) can be simplified to the linear circuit shown in Fig. 3(c), which is similar to the unidirectional circuit shown in Fig. 1(b). Similarly, in the second half of each cycle when V_{oc} is decreasing, the circuit can also be simplified, but the direction of C_L is reversed because of the function of the full-bridge rectifier.

The initial condition we utilized is still the same with the analysis of unidirectional charging, that is the initial charges on both C_T and C_L are zero. So at the beginning of the first cycle, the total charges stored on node M [shown in Fig. 3(b) and (c)] are zero, which is shown in mathematics as $Q_1^M = 0$ (Q_k^M stands for the total charges on the node M at the beginning of the kth cycle).

Now, we consider the kth charging cycle. During its first half, it is a unidirectional charging step. Similar to the previous derivation, at the end of this half cycle ($x = x_{\max}$), the charges stored on $C_T(Q)$ and $C_L(Q^C)$ can be given by

$$Q_{k,1\mathrm{end}} = \frac{C_L Q_{\mathrm{SC,max}} - C_{\min} Q_k^M}{C_L + C_{\min}} \tag{7}$$

$$Q_{k,1\mathrm{end}}^C = C_L \frac{Q_{\mathrm{SC,max}} + Q_k^M}{C_L + C_{\min}} \tag{8}$$

where the subscript in $Q_{k,1\mathrm{end}}$ stands for its value at the end of the 1st half in the kth charging cycle and $C_{\min}$ stands for the value of $C_T(x = x_{\max})$.

From the end of the first half cycle to the beginning of the second half cycle, the direction of C_L is reversed due to the function of the full-bridge rectifier. Thus, the charges stored on Node M at the beginning of the second half of the kth cycle ($Q_{k,\mathrm{mid}}^M$) can be given by

$$Q_{k,\mathrm{mid}}^M = -Q_{k,2\mathrm{begin}} + Q_{k,2\mathrm{begin}}^C = -Q_{k,1\mathrm{end}} - Q_{k,1\mathrm{end}}^C. \tag{9}$$

The second half cycle is also a unidirectional charging step (x is from $x_{\max}$ back to 0). Similar to the previous derivation, at the end of this half cycle ($x = 0$), the charges stored on $C_T(Q)$ and $C_L(Q^C)$ can be obtained as [$C_{\max}$ stands for the value of $C_T(x = 0)$]

$$Q_{k,2\mathrm{end}} = -\frac{C_{\max} Q_{k,\mathrm{mid}}^M}{C_L + C_{\max}} \tag{10}$$

$$Q_{k,2\mathrm{end}}^C = \frac{C_L Q_{k,\mathrm{mid}}^M}{C_L + C_{\max}}. \tag{11}$$

At the end of this second half-cycle, the direction of C_L is reversed again. Thus, the charges stored on Node M at the beginning of the $(k+1)$th cycle (Q_{k+1}^M) can be given by

$$Q_{k+1}^M = -Q_{k+1,1\mathrm{begin}} + Q_{k+1,1\mathrm{begin}}^C = -Q_{k,2\mathrm{end}} - Q_{k,2\mathrm{end}}^C. \tag{12}$$

Through the above equations, a recursion relationship for Q_k^M can be derived below

$$Q_{k+1}^M = \frac{C_L - C_{\max}}{C_L + C_{\max}} \frac{C_L - C_{\min}}{C_L + C_{\min}} Q_k^M + 2\frac{C_L - C_{\max}}{C_L + C_{\max}} \frac{C_L}{C_L + C_{\min}} Q_{\mathrm{SC,max}}. \tag{13}$$

With the boundary condition of $Q_1^M = 0$, the above recursion relationship can be easily solved as

$$Q_k^M = \frac{C_L - C_{\max}}{C_{\min} + C_{\max}} Q_{\mathrm{SC,max}} - \frac{C_L - C_{\max}}{C_{\min} + C_{\max}} Q_{\mathrm{SC,max}} \times \left[\frac{(C_L - C_{\max})(C_L - C_{\min})}{(C_L + C_{\max})(C_L + C_{\min})}\right]^{k-1}. \tag{14}$$

Therefore, the voltage on C_L at the end of kth charging cycle ($|V_{k,2\mathrm{end}}^C|$) can be easily derived as

$$\left|V_{k,2\mathrm{end}}^C\right| = \frac{Q_{\mathrm{SC,max}}}{C_{\min} + C_{\max}} \left\{1 - \left[1 - \frac{2(C_{\min} + C_{\max})C_L}{(C_L + C_{\max})(C_L + C_{\min})}\right]^k\right\}. \tag{15}$$

It is useful to note that the above derivation is also applicable to other categories of TENGs because we did not utilize any TENG category information in our derivation. In practical applications, C_L is usually much larger than both $C_{\max}$ and $C_{\min}$. Under this condition, (15) can be further simplified to (where f stands for the frequency of the periodic motion)

$$\left|V_{k,2\mathrm{end}}^C\right| = \frac{Q_{\mathrm{SC,max}}}{C_{\min} + C_{\max}} \left\{1 - \exp\left[-\frac{2(C_{\min} + C_{\max})k}{C_L}\right]\right\} = \frac{Q_{\mathrm{SC,max}}}{C_{\min} + C_{\max}} \left\{1 - \exp\left[-\frac{2(C_{\min} + C_{\max})ft}{C_L}\right]\right\}. \tag{16}$$

Equation (16) clearly shows that a TENG together with a bridge rectifier under periodic external motion is completely comparable to a dc voltage source in series with a resistor regarding the capacitor charging characteristics. They all follow the same exponential saturation trend. The value of the

dc source is the saturation voltage (V_{sat}) shown in Fig. 4(a) and its value can be easily calculated as

$$V_{\text{sat}} = \lim_{k\to\infty} \left|V_{k,2\text{end}}^{C}\right| = \frac{Q_{\text{SC,max}}}{C_{\text{min}} + C_{\text{max}}}. \tag{17}$$

Similar to the first-order RC charging circuit, V_{sat} is only a function of TENG parameters, but it is independent of C_L, which is consistent with the numerical results shown in Fig. 4(a). Utilizing the parameters shown in Table II, we can calculate that the saturation voltage for the previous TENG system is 105.06 V, which is very close to the simulation results (104.8 V).

In addition to the saturation voltage, the charging speed is another important charging parameter. Analogous to a first-order RC charging circuit, time constant (τ) is utilized to characterize the charging speed, which can be easily given by

$$\tau = \frac{C_L}{2(C_{\text{min}} + C_{\text{max}})f}. \tag{18}$$

The time constant is directly proportional to C_L. Therefore, the value of the effective resistor in the first-order RC charging circuit can be easily extracted as $1/[2f(C_{\text{max}} + C_{\text{min}})]$, which shows that the TENG with a larger inherent capacitance can charge C_L with a higher speed.

Moreover, when C_L is large enough, linear charging behavior is observed and the TENG is working on quasi-SC condition. When C_L is close to infinity, the final stored charges at the end of the kth charging cycle can be given by

$$\lim_{C_L\to\infty} \left|V_{k,2\text{end}}^{C}\right| = \lim_{C_L\to\infty} \frac{2kQ_{\text{SC,max}}}{C_L} = 0 \tag{19}$$

$$\lim_{C_L\to\infty} \left|Q_{k,2\text{end}}^{C}\right| = C_L \lim_{C_L\to\infty} \left|V_{k,2\text{end}}^{C}\right| = 2kQ_{\text{SC,max}}. \tag{20}$$

Since the maximum charge generated from the TENG is $Q_{\text{SC,max}}$ for each half cycle, the above results show that all the charges generated from the TENG are stored in C_L. At the same time, the voltage difference across the TENG is zero, which is completely consistent with the numerical results shown in Fig. 4(b).

Finally and most importantly, there also exists an optimum load capacitance ($C_{L,\text{opt}}$) at which the stored energy reaches its maximum value. This optimum load capacitance is critically important for optimized design for such energy harvesting system and needs to be analytically derived to show its dependence on the TENG structural parameters and cycle numbers.

From (16), the energy stored in the load capacitor at the end of the kth charging cycle ($E_{k,\text{end}}^{C}$) is given by

$$E_{k,\text{end}}^{C} = \frac{C_L\left(V_{k,2\text{end}}^{C}\right)^2}{2} = \frac{C_L(Q_{\text{SC,max}})^2}{2(C_{\text{min}} + C_{\text{max}})^2} \times \left\{1 - \exp\left[-\frac{2(C_{\text{min}} + C_{\text{max}})k}{C_L}\right]\right\}^2. \tag{21}$$

At the optimum capacitance, $E_{k,\text{end}}^{C}$ reaches its maximum value. Therefore

$$\left(\frac{dE_{k,\text{end}}^{C}}{dC_L}\right)_{C_L=C_{L,\text{opt}}} = 0. \tag{22}$$

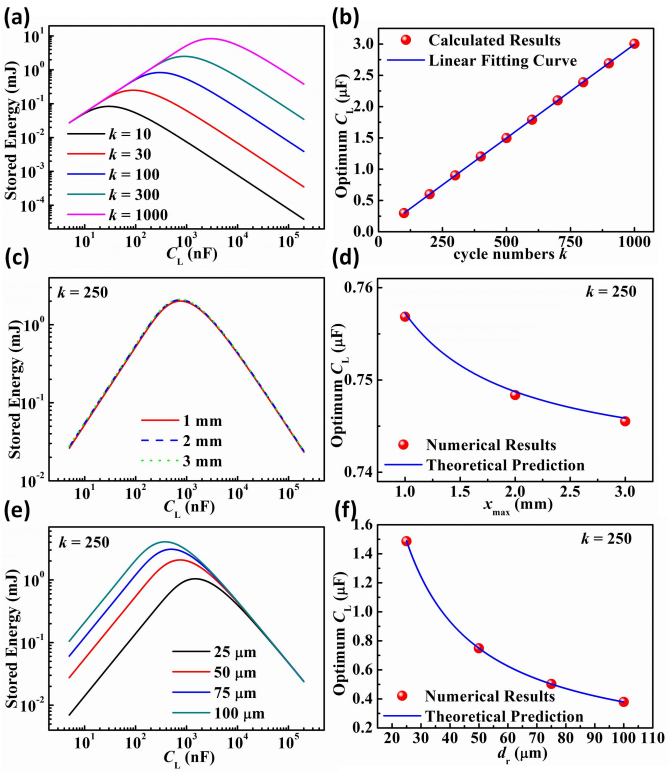

Fig. 5. Analysis of the optimum load capacitance. (a) Relationship between stored energy and load capacitance at different cycle numbers. (b) Extracted optimum capacitance with cycle numbers. (c) Relationship between stored energy and load capacitance at different x_{max}. (d) Extracted optimum capacitance with x_{max}. (e) Relationship between stored energy and load capacitance at different d_r. (f) Extracted optimum capacitance with d_r.

Thus, an analytical solution for $C_{L,\text{opt}}$ can be obtained as

$$C_{L,\text{opt}} = 1.592k(C_{\text{min}} + C_{\text{max}}). \tag{23}$$

Equation (23) is an excellent approximation of $C_{L,\text{opt}}$ only when k is >10 because the approximation that C_L is much larger than both C_{max} and C_{min} is utilized during the derivation of (16). However, the charging cycle number in almost all cases is >10, so (23) is always a good estimation in practical applications.

To verify the above theoretical anticipations, numerical calculations are carried out with contact-mode attached-electrode TENGs with different parameters and cycle numbers, as shown in Fig. 5. Without special notation in the figure, the values utilized for the parameters are exactly the same as those in Table II. First, the influence of the charging cycle number on $C_{L,\text{opt}}$ is investigated. As shown in Fig. 5(a) and (b), when the number of charging cycles increases, $C_{L,\text{opt}}$ and the maximum energy stored both increases and an accurately linear trend between $C_{L,\text{opt}}$ and the charging cycle numbers is observed. In addition, the influence of several structural parameters on $C_{L,\text{opt}}$ is investigated as well. For practical contact-mode TENGs with an acceptable charge generation efficiency (x_{max} should be much larger than d_0) shown in Fig. 3(a) [21], (23) can be further simplified utilizing the parallel plate capacitance model

$$C_{L,\text{opt}} = 1.592k\left(\frac{\varepsilon_0 S}{d_0 + x_{\text{max}}} + \frac{\varepsilon_0 S}{d_0}\right) \approx \frac{1.592k\varepsilon_0 S}{d_0}. \tag{24}$$

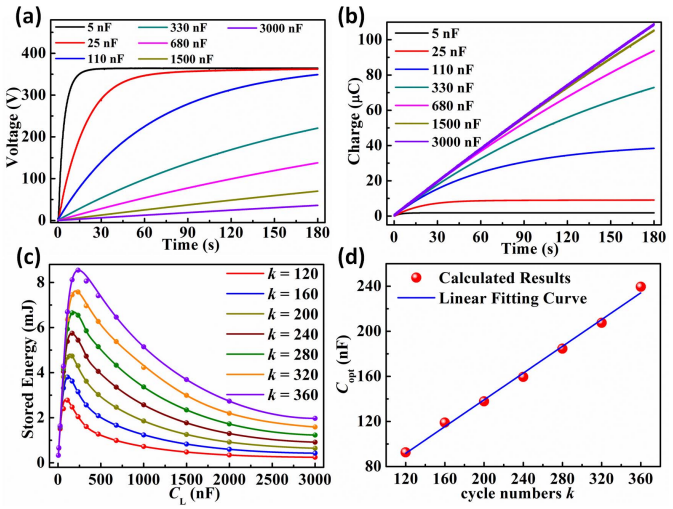

Fig. 6. Experimental measured TENG charging profiles under periodic motion. (a) Measured voltage–time relationship at different load capacitances. (b) Measured stored charge–time relationship at different load capacitances. (c) Measured stored energy–load capacitance relationship at different cycle numbers. (d) Extracted optimum capacitance with cycle numbers.

First, we investigate the influence of $x_{\max}$. Intuitively, increasing this maximum moving distance will increase the OC voltage of the TENG [21] and may have an obvious influence on V_{sat} and $C_{L,\text{opt}}$. However, from (16), V_{sat} and $C_{L,\text{opt}}$ are mainly affected by the sum of $C_{\min}$ and $C_{\max}$, in which $C_{\min}$ is negligible compared with $C_{\max}$ for a contact-mode attached-electrode TENG [21]. Thus, since $x_{\max}$ can only affect $C_{\min}$, the whole charging behavior and $C_{L,\text{opt}}$ is almost independent of $x_{\max}$. As shown in Fig. 5(c), the total stored energy as a function of C_L for different $x_{\max}$ almost coincide with each other. When $x_{\max}$ increases from 1 to 3 mm, $C_{L,\text{opt}}$ only decreases from 756.9 to 745.5 nF, which is completely consistent with the theoretical estimation from (24). In contrast with $x_{\max}$, since the dielectric thickness (d_r) will have significant impact on $C_{\max}$, the total charging behavior and $C_{L,\text{opt}}$ is obviously dependent on d_r. As shown in Fig. 5(e) and (f), when d_r increases from 25 to 100 μm, the maximum stored energy increases from 1.04 to 4.05 mJ and $C_{L,\text{opt}}$ decreases from 1486 to 379 nF, which is completely consistent with the theoretical inverse ratio relationship.

To further validate the theoretical equation presented above, experiments were carried out to compare with the theoretical expectations. A contact-mode attached-electrode TENG with the structure shown in Fig. 3(a) was utilized in this experiment. The triboelectric pair material in the TENG was Al and polytetrafluoroethylene (PTFE). Al was utilized as one electrode and at the backside of the PTFE, copper was deposited as another electrode. The whole structure was supported by two acrylic sheets. The bottom plate was bonded onto the measurement desk and the top plate was driven by a motor with a 2-Hz harmonic motion. Through bridge rectifier made from four low-leakage and high-breakdown diodes, different low-leakage capacitors were charged by this TENG and a voltage-meter (Keithley Model 6514) was utilized to measure the real-time voltage across the load capacitor. The measured charging curves for different capacitors are shown in Fig. 6(a) and (b), which have the same shape and trend as the theoretical prediction shown in Fig. 4. The relationship between the stored energy and the load capacitance is also plotted and an optimum capacitance for the maximized stored energy is also observed as the theoretical prediction. If the interpolated optimum capacitance was extracted and plotted with the cycle number, a very good linear relationship is observed, which is consistent with our theoretical prediction. All of the above experimental results further validate the conclusions from our theoretical derivation, clearly showing its potential to guide future experimental designs.

IV. Conclusion

A comprehensive theoretical study of the charging behavior of TENGs is presented for the first time. The charging behavior strongly depends on the load capacitance. For multicycle charging with a bridge rectifier, the saturation charging behavior is completely analogous to utilizing a dc voltage source with an internal resistance to charge a load capacitor. The TENG with larger SC transferred charges and smaller inherent TENG capacitance can charge a load capacitor to a higher saturation voltage under unlimited charging cycles and the TENG with larger inherent capacitance can provide a smaller charging time constant. An optimum load capacitance that matches the TENGs impedance is observed for the maximum stored energy. This optimum load capacitance is linearly proportional to the charging cycle numbers and the inherent capacitance of the TENG. Experiments were performed to further validate our theoretical anticipation. This paper clearly shows the unique TENG charging characteristics, which can serve as an important guidance to design an integrated TENG energy harvesting system for practical application.

References

[1] S. P. Beeby *et al.*, "A micro electromagnetic generator for vibration energy harvesting," *J. Micromech. Microeng.*, vol. 17, no. 7, pp. 1257–1265, Jul. 2007.

[2] C. R. Saha, T. O'Donnell, N. Wang, and P. McCloskey, "Electromagnetic generator for harvesting energy from human motion," *Sens. Actuators A, Phys.*, vol. 147, no. 1, pp. 248–253, Sep. 2008.

[3] Y. Suzuki, "Recent progress in MEMS electret generator for energy harvesting," *IEEJ Trans. Electr. Electron. Eng.*, vol. 6, no. 2, pp. 101–111, Mar. 2011.

[4] H.-W. Lo and Y.-C. Tai, "Parylene-based electret power generators," *J. Micromech. Microeng.*, vol. 18, no. 10, p. 104006, Oct. 2008.

[5] O. D. Jefimenko and D. K. Walker, "Electrostatic current generator having a disk electret as an active element," *IEEE Trans. Ind. Appl.*, vol. 14, no. 6, pp. 537–540, Nov. 1978.

[6] P. D. Mitcheson, P. Miao, B. H. Stark, E. M. Yeatman, A. S. Holmes, and T. C. Green, "MEMS electrostatic micropower generator for low frequency operation," *Sens. Actuators B, Phys.*, vol. 115, nos. 2–3, pp. 523–529, Sep. 2004.

[7] Y. Tada, "Experimental characteristics of electret generator, using polymer film electrets," *Jpn. J. Appl. Phys.*, vol. 31, no. 3, pp. 846–851, Mar. 1992.

[8] A. Khaligh, P. Zeng, and C. Zheng, "Kinetic energy harvesting using piezoelectric and electromagnetic technologies-state of the art," *IEEE Trans. Ind. Electron.*, vol. 57, no. 3, pp. 850–860, Mar. 2010.

[9] R. G. Horn, D. T. Smith, and A. Grabbe, "Contact electrification induced by monolayer modification of a surface and relation to acid–base interactions," *Nature*, vol. 366, no. 6454, pp. 442–443, Dec. 1993.

[10] H. T. Baytekin, A. Z. Patashinski, M. Branicki, B. Baytekin, S. Soh, and B. A. Grzybowski, "The mosaic of surface charge in contact electrification," *Science*, vol. 333, no. 6040, pp. 308–312, Jul. 2011.

[11] L. S. McCarty and G. M. Whitesides, "Electrostatic charging due to separation of ions at interfaces: Contact electrification of ionic electrets," *Angew. Chem. Int. Ed.*, vol. 47, no. 12, pp. 2188–2207, 2008.
[12] F.-R. Fan, Z.-Q. Tian, and Z. L. Wang, "Flexible triboelectric generator," *Nano Energy*, vol. 1, no. 2, pp. 328–334, Mar. 2012.
[13] S. Wang *et al.*, "Motion charged battery as sustainable flexible-power-unit," *Acs Nano*, vol. 7, no. 12, pp. 11263–11271, Dec. 2013.
[14] X.-S. Zhang *et al.*, "Frequency-multiplication high-output triboelectric nanogenerator for sustainably powering biomedical microsystems," *Nano Lett.*, vol. 13, no. 3, pp. 1168–1172, Mar. 2013.
[15] Y. S. Zhou *et al.*, "Nanometer resolution self-powered static and dynamic motion sensor based on micro-grated triboelectrification," *Adv. Mater.*, vol. 26, no. 11, pp. 1719–1724, Mar. 2014.
[16] S. Kim *et al.*, "Transparent flexible graphene triboelectric nanogenerators," *Adv. Mater.*, vol. 26, no. 23, pp. 3918–3925, Jun. 2014.
[17] S. M. Niu *et al.*, "Theoretical investigation and structural optimization of single-electrode triboelectric nanogenerators," *Adv. Funct. Mater.*, vol. 24, no. 22, pp. 3332–3340, Jun. 2014.
[18] S. Niu *et al.*, "Simulation method for optimizing the performance of an integrated triboelectric nanogenerator energy harvesting system," *Nano Energy*, vol. 8, pp. 150–156, Sep. 2014.
[19] S. Niu *et al.*, "Theory of sliding-mode triboelectric nanogenerators," *Adv. Mater.*, vol. 25, no. 43, pp. 6184–6193, Nov. 2013.
[20] S. Niu *et al.*, "A theoretical study of grating structured triboelectric nanogenerators," *Energy Environ. Sci.*, vol. 7, no. 7, pp. 2339–2349, Jul. 2014.
[21] S. Niu *et al.*, "Theoretical study of contact-mode triboelectric nanogenerators as an effective power source," *Energy Environ. Sci.*, vol. 6, no. 12, pp. 3576–3583, Dec. 2013.

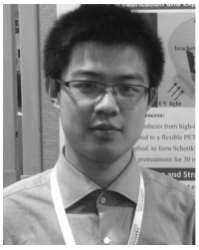

Simiao Niu received the B.E. (Hons.) degree in microelectronics from Tsinghua University, Beijing, China, in 2011. He is currently pursuing the Ph.D. degree with the School of Materials Science and Engineering, Georgia Institute of Technology, Atlanta, GA, USA, under the supervision of Prof. Z. L. Wang. His current research interests include theoretical and experimental studies on: mechanical energy harvesting by nanogenerators and high-performance sensors based on piezoelectric nanowires.

Ying Liu received the B.S. degree in physics from Peking University, Beijing, China, in 2009, and the Ph.D. degree in materials science and engineering from the Georgia Institute of Technology, Atlanta, GA, USA, in 2014. She is a Post-Doctoral Researcher under the supervision of Prof. Z. L. Wang. Her current research interests include theory and experiments of piezotronics and piezo-phototronics, theory of triboelectric generators, hybrid LEDs, and hybrid energy harvesting devices.

Yu Sheng Zhou received the B.S. degree in applied physics and the M.S. degree in optics from Beihang University, Beijing, China. He is currently pursuing the Ph.D. degree with the School of Materials Science and Engineering, Georgia Institute of Technology, Atlanta, GA, USA. His current research interests include MEMS sensors, energy harvesting devices, and scanning probe microscopic characterization of functional materials.

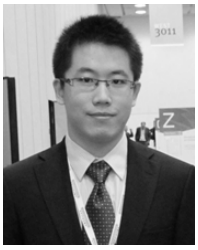

Sihong Wang received the Ph.D. degree in materials science and engineering from the Georgia Institute of Technology, Atlanta, GA, USA, in 2014, under the supervision of Prof. Z. L. Wang.

He is currently a Post-Doctoral Fellow with the Prof. Z. L. Wang Group, Georgia Institute of Technology. His current research interests include nanomaterial-based mechanical energy harvesting and energy storage, self-powered systems, and nanogenerator-based sensors.

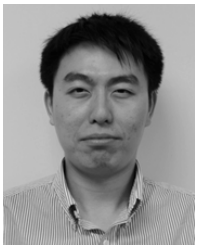

Long Lin received the B.S. degree in materials science and engineering from Tsinghua University, Beijing, China, in 2010. He is currently pursuing the Ph.D. degree with the Georgia Institute of Technology, Atlanta, GA, USA, under the supervision of Prof. Z. L. Wang. His current research interests include synthesis of semiconductor nanomaterials, piezoelectric nanogenerators, triboelectric nanogenerators, self-powered systems, and active sensors.

Zhong Lin Wang is currently a Hightower Chair and Regents's Professor with the Georgia Institute of Technology, Atlanta, GA, USA, and the Chief Scientist and a Director with the Beijing Institute of Nanoenergy and Nanosystems, Chinese Academy of Sciences, Beijing, China. His discovery and breakthroughs in developing nanogenerators established the principle and technological road map for harvesting mechanical energy from environment and biological systems for powering personal electronics.